Frequency and Phase Calculation Method of Rotating Machinery Vibration Signal Based on Adaptive Notch Filter

Xudong Guan, Hao Peng, Sihan Yu and Lidong Sun

School of Mechanical Engineering and Rail Transit, Changzhou University, Changzhou, China.
E-mail: guanxd@cczu.edu.cn

(Received 2 November 2025; accepted 3 March 2026)

In the field of rotating machinery, rotor vibration is an important issue. The most common vibration signal is sinusoidal. Only by accurately identifying the frequency and phase can the vibration be effectively suppressed. For the problem of solving the frequency and phase of rotating machinery vibration signals, a solver is constructed based on an adaptive notch filter (ANF), realizing the solution of frequency and phase of vibration signals. Firstly, the basic principle of ANF is introduced, and the frequency and phase solvers are constructed. Secondly, the influence of ANF parameters on the solution is analyzed. Finally, simulated and experimental signals are used to verify the method. The results show that the method can accurately solve the frequency and phase of sinusoidal signals and achieve zero error for simulated signals. For experimental signals, there is a small deviation from the theoretical value, which may be caused by factors such as sensor installation angle and mechanical assembly.

1. INTRODUCTION

In the field of rotating machinery such as motor, generator and blower, rotor vibration signal and rotor centrifugal force signal are usually used as the analytical factors to evaluate system performance. Among these signals, sinusoidal signals are the most common. As the important criteria of sinusoidal signal, frequency and phase play an important role in the suppression of vibration and the improvement of the dynamic performance of the rotor system. Therefore, it is particularly important to be able to accurately identify the frequency and phase of a sinusoidal signal.

To solve the problem of frequency and phase of sinusoidal signal, many researchers have done a lot of research in related fields and proposed many solutions. Alegria et al. analyzed the mechanism of phase noise on the initial phase estimation of sinusoidal signal of known frequencies.[1] And they discussed how phase noise causes deviation in the initial phase estimation through theoretical derivation and mathematical analysis. Yang et al. proposed an improved multi-order Kalman filter.[2] Since the cosine and sinusoidal components are separated, the filter performance is improved, which makes the recognition and tracking of complex signals possible. However, this method relies on accurate model parameters. If the model parameters are set improperly, the filtering effect may be affected. Miao et al. proposed a new adaptive filter structure.[3] Based on the adaptive algorithm, the filter can adjust the parameters in real time to adapt to the changing characteristics of the signal. However, this method is sensitive to initial conditions. The performance of the filter may be affected by the initial conditions, and resulting in unstable performance in some cases. Duan et al. focused on improving the analysis of rotating machinery signals through time-varying filtering techniques for effective fault diagnosis under complex and dynamic operating conditions.[4] But this approach requires high computing resources, especially in the case of real-time monitoring, which can lead to system delays. Saber et al. proposed a frequency estimation method based on deep learning, which can accurately estimate the frequency of unknown input signals.[5] However, the performance of this method is highly dependent on the quality and quantity of the training data. Singh et al. developed a frequency and phase estimation method based on nonlinear least squares.[6] The validity of the proposed method is verified by using different test data sets. However, this method may not perform as well as other algorithms with better robustness in the face of high-noise environments. Guan et al. proposed a surge frequency detection method for magnetic suspension fluid machinery based on second order generalized integrator-frequency locked loop with prefilter.[7,8] But the above surge detection method does not involve solving the phase of the signal. Magron et al. proposed an online spectrum inversion algorithm.[9] By using deep learning methods for low phase lag reconstruction, it is particularly suitable for real-time audio signal processing. This approach performs well in terms of signal quality and computational efficiency. Mayer et al. proposed a single channel speech separation method based on time frequency mask, which improved the accuracy of speech separation by estimating alternating current phase information.[10] In summary, researchers have proposed more frequency and phase solutions. However, most methods have problems such as large computation, complex algorithms, high data quality dependence and poor real-time computation.

The method based on adaptive notch filter has the characteristics of simple implementation,[11,12] high precision and fast response, so it is widely used in sinusoidal signal recognition. Therefore, this paper uses ANF to solve the frequency and phase of rotating machinery vibration signal, which provides a new idea for the analysis and suppression of rotating machinery vibration signal.

The rest of this paper is arranged as follows. The second part introduces the basic principle of ANF and constructs a frequency-phase solver based on ANF. The third part analyzes

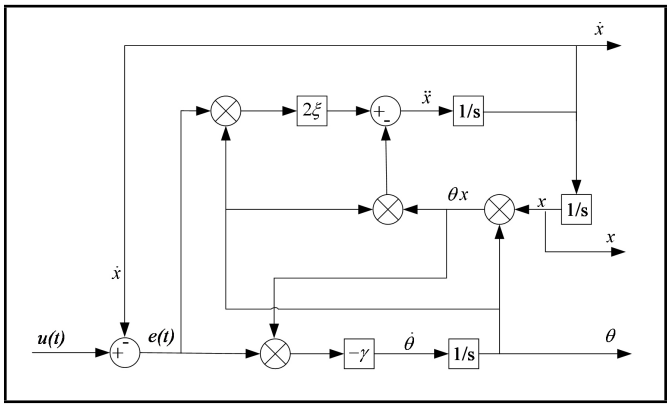

Figure 1. ANF principal block diagram.

the parameters influence of ANF on the solution of frequency and phase. In the fourth part, the frequency and phase of a single sinusoidal signal are simulated. Additionally, the frequencies and phase differences of two sinusoidal signals are also simulated. The fifth part is the experimental research. The conclusion is in the last part.

2. FREQUENCY AND PHASE SOLUTION METHODS

2.1. Principle of ANF

Equation (1) is a sinusoidal signal with unknown parameters, where A is the amplitude of a single signal, ω is the frequency of the sinusoidal signal, and φ is the initial phase of the sinusoidal signal:

$$u(t) = A\sin(\omega t + \varphi); \tag{1}$$

The unknown signal can be tracked in real time by the ANF method to obtain signal parameters. Equation (2) is the differential equation of ANF:[13,14]

$$\begin{cases} \ddot{x} + \theta^2 x = 2\xi\theta e(t); \\ \dot{\theta} = -\gamma x\theta e(t); \\ e(t) = u(t) - \dot{x}. \end{cases} \tag{2}$$

In the equation, θ is the estimated frequency of $u(t)$, which is equal to the actual frequency ω of $u(t)$. $\dot{x}$ is the instantaneous value of $u(t)$. ξ and γ are the ANF parameters, which determine the steady state accuracy and convergence rate of the ANF respectively.

When $u(t)$ only contains the fundamental wave component, then Eq. (2) has the following unique solution:

$$\begin{bmatrix} x \\ \dot{x} \\ \theta \end{bmatrix} = \begin{bmatrix} -\dfrac{A}{\omega}\cos(\omega t + \varphi) \\ A\sin(\omega t + \varphi) \\ \omega \end{bmatrix}. \tag{3}$$

Figure 1 shows the internal schematic diagram of ANF corresponding to Eqs. (2) and (3). In Fig. 1, the orthogonal signal $-\theta x$ can be calculated from the solved x and θ.

For a multi-span rotors system with couplings, the rotor vibration signal may also contain harmonic components of the rotational frequency, such as twice and three times the rotational frequency.[15] Multiple adaptive notch filters can be used in parallel to extract each harmonic and its quadrature component.

The input signal is as follows:

$$u'(t) = \sum_{h=1}^{n} A_h \sin(\omega_h t + \varphi_h); \tag{4}$$

Among them, h represents the harmonic order. The ANF differential equation is transformed into a new system of differential equation as follows:[16]

$$\begin{cases} \ddot{x_h} + h^2\theta^2 x_h = 2\xi\theta e(t); \\ \dot{\theta} = -\gamma x_1 \theta e(t); \\ e(t) = u'(t) - \sum_{h=1}^{n} \dot{x_h}. \end{cases} \tag{5}$$

The solution of ANF is as follows:

$$\begin{bmatrix} x_h \\ \dot{x}_h \\ \theta \end{bmatrix} = \begin{bmatrix} -\dfrac{A_h}{h\omega_1}\cos(h\omega_1 t + \varphi_h) \\ A_h \sin(h\omega_1 t + \varphi_h) \\ \omega_1 \end{bmatrix}. \tag{6}$$

As shown in Fig. 2 is the principal block diagram of multi-harmonic signal tracking based on Eqs. (5) and (6).

2.2. Frequency and Phase Solution Based on ANF

Based on the ANF method, the frequency and phase of the sinusoidal signal can be solved. Figure 3(a) is a schematic block diagram of the solution method. In Fig. 3(a), the tracking result of the input signal $u(t)$ is $\dot{x}$. It can be seen from Eq. (3) that $-\theta x$ is $A\cos(\omega t + \varphi)$, and which is the orthogonal signal of the input signal.

θ is the estimated frequency of $u(t)$, which is equal to the actual frequency ω of $u(t)$. The phase $\omega t + \varphi$ can be calculated by Eq. (7), where φ is the initial phase of the input signal:

$$\omega t + \varphi = \arctan\left(\frac{A\sin(\omega t + \varphi)}{A\cos(\omega t + \varphi)}\right). \tag{7}$$

It is obvious that the method shown in Fig. 3(b) can be used to solve the phase difference of the two signals. One cycle of the rotor is 2π. After transformation, the range of the rotor phase in this paper is taken as $[-\pi, \pi]$.

3. PARAMETERS INFLUENCE OF ANF

The essence of ANF is to accurately track the input signal, to obtain the frequency and phase of the tracking signal. Real-time and accurate tracking of the input signal is an important factor in calculating the parameters of the input signal. The following is the research and analysis of ANF parameters γ and ξ.

3.1. Influence of Parameter γ on Signal Tracking

Many systems have high requirements for the real-time performance of signal recognition, such as rotating machinery systems like active magnetic bearing and electric motors. It is necessary to identify the basic information of the signal in a timely manner after the system responds. The parameter γ in

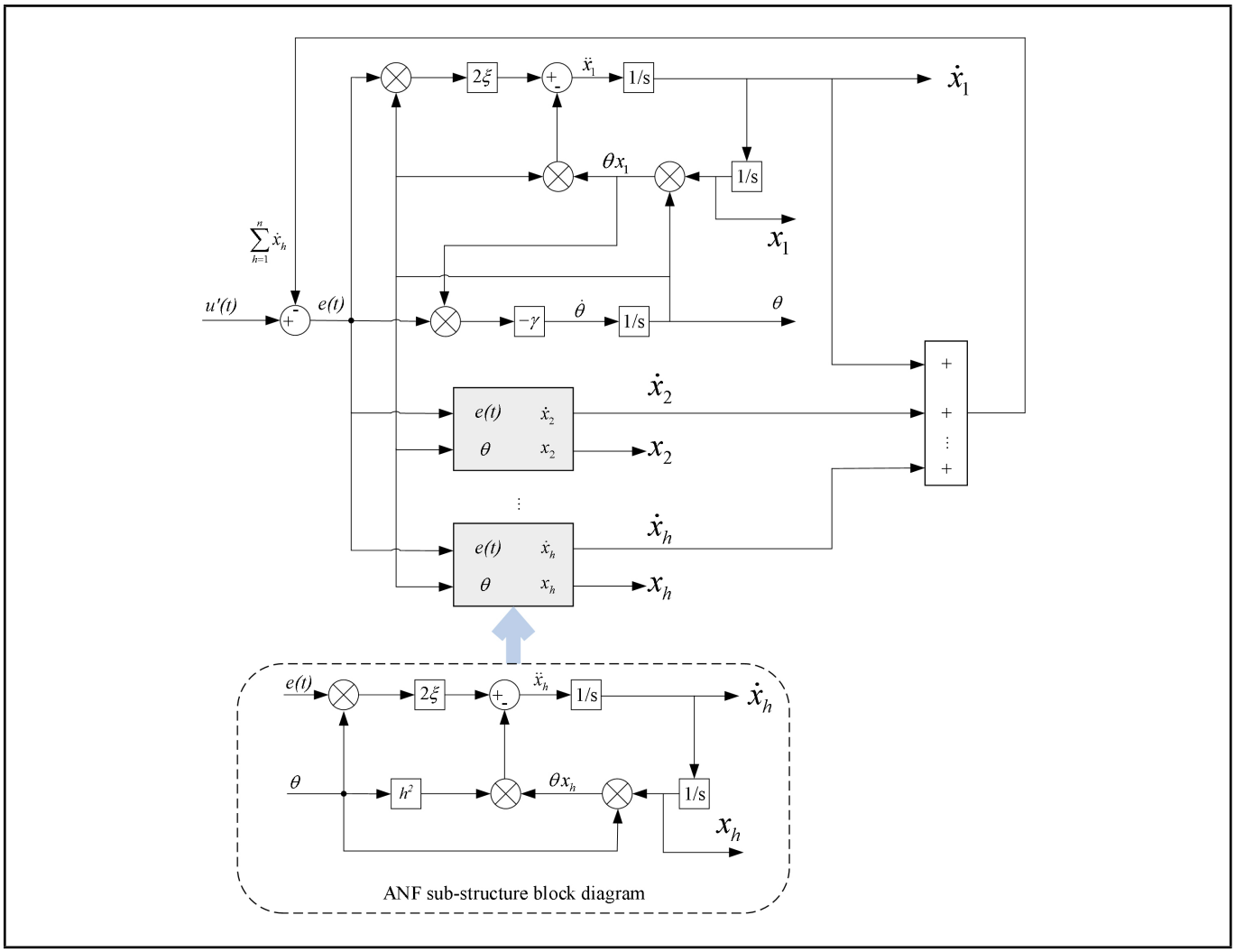

Figure 2. Principal block diagram of multi-harmonic signal tracking.

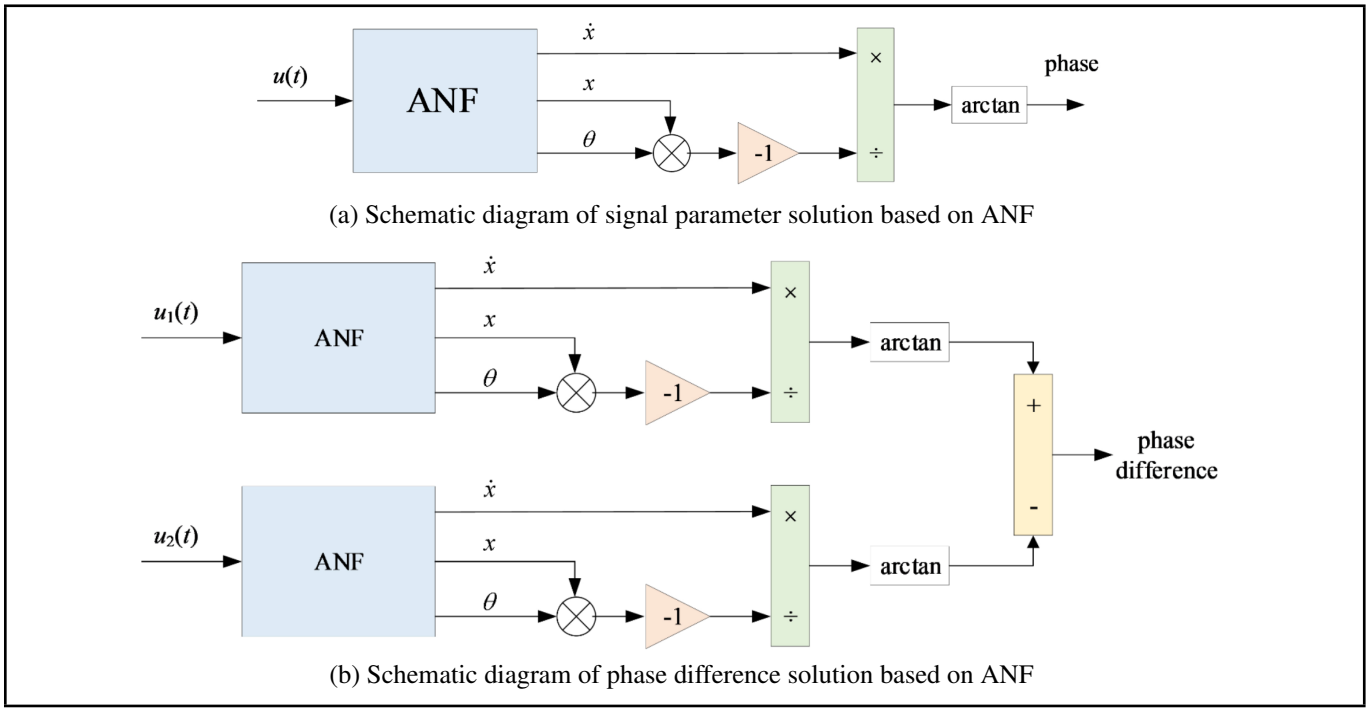

Figure 3. Principle of solving system parameters and phase difference based on ANF.

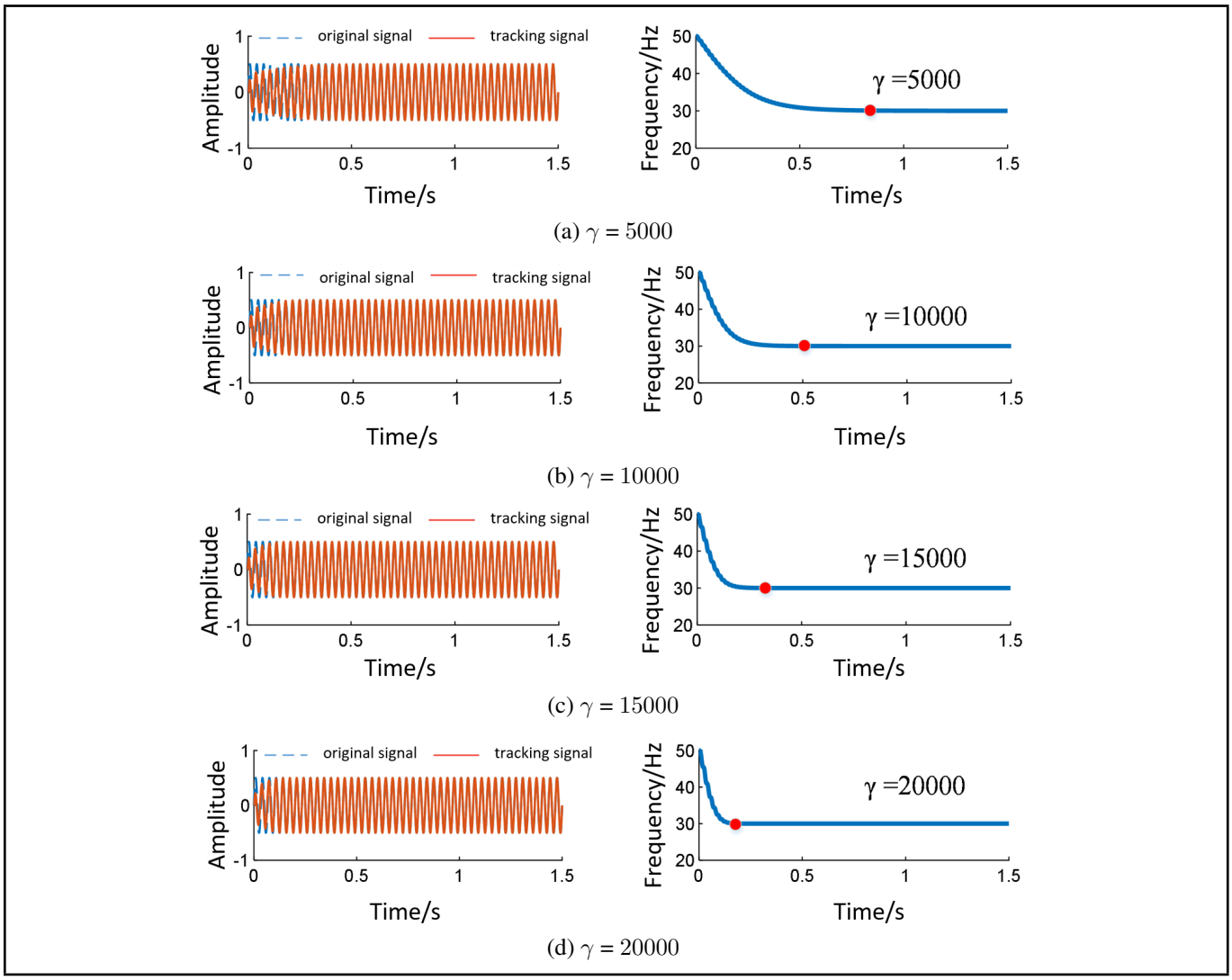

Figure 4. Comparison of signal tracking and frequency recognition results under different γ.

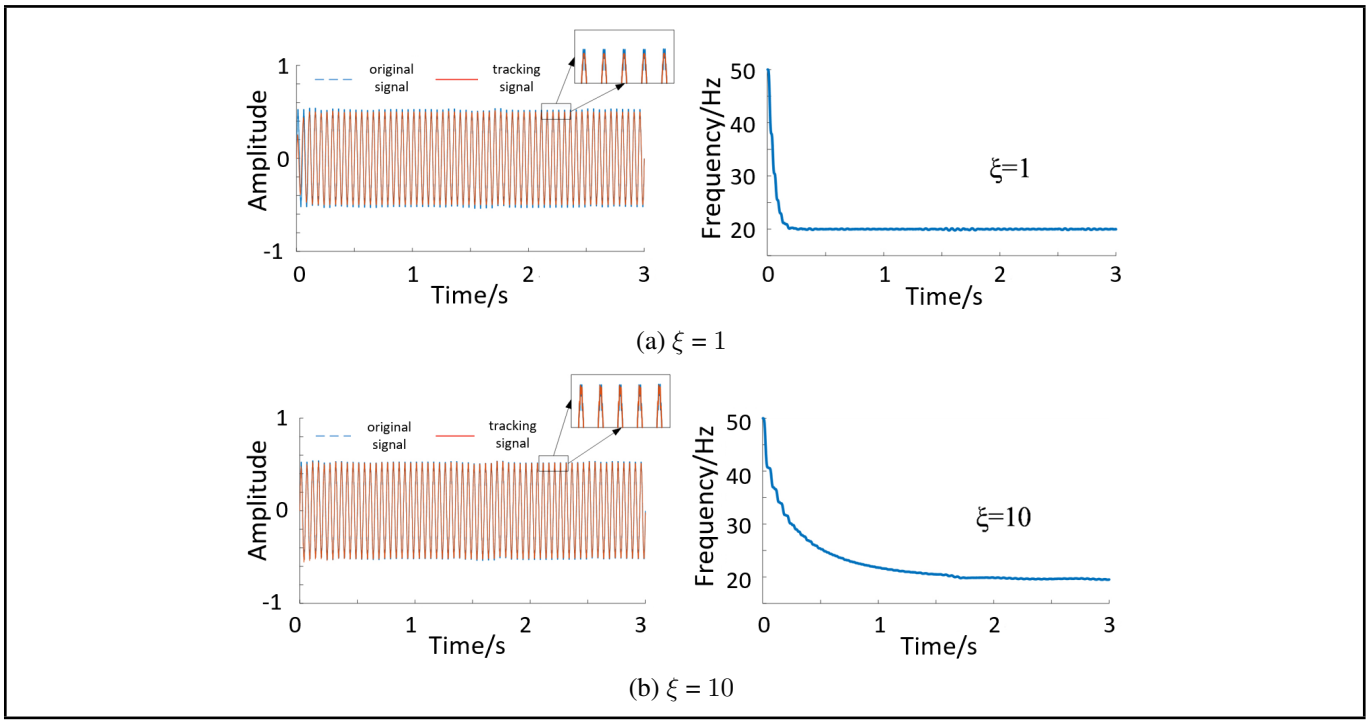

Figure 5. Comparison of signal tracking and frequency recognition results under different ξ.

ANF is the convergence speed gain coefficient, which affects the recognition speed of ANF system. Therefore, a mathematical model was built, and the influence of parameter γ on the system was analyzed.

Suppose the signal $u(t)$ to be measured is $0.5 \times \sin(30 \times 2\pi t)$. In the system, the initial value of ω is 50 Hz. γ takes 5000, 10000, 15000 and 20000 respectively. The simulation results are shown in Fig. 4. The original signal and the tracking signal under different parameters are compared respectively. After the identification frequency stabilizes at 30 Hz, the tracking signal basically coincides with the original signal without phase lead or phase lag.

From Fig. 4, it can be concluded that when the value of γ gradually increases, the convergence speed of the system gradually increases, and the corresponding recognition speed also gradually increases. When the parameter γ is set to 20000, the accurate acquisition of signal information is achieved in about 0.2 s. Therefore, for detection systems with different requirements, choose the appropriate parameters to achieve accurate identification.

3.2. Influence of Parameter ξ on Signal Tracking

In addition to tracking speed, tracking accuracy is also one of the important factors for performance of ANF. In a signal system with multiple harmonics and noise characteristics, only by accurately tracking the signal can its frequency be accurately solved. The parameter ξ determines the notch width in the ANF, thus affecting the accuracy of the system in tracking signals. The following is an analysis of different parameters ξ.

Take the original signal $u(t)$ as $0.5 \times \sin(30 \times 2\pi t)$. To compare the precision of signal tracking under different parameters, high-frequency harmonics and white noise were added to the input signal. In the system, the initial value of ω is 50 Hz. γ was taken as 20000, and ξ takes 1 and 10 respectively. The simulation results are shown in Fig. 5, which compares the tracking effect of the system on the original signal under different parameters. As can be seen from Fig. 5, the tracking effect of the system on the original signal can be improved when the value of ξ is increased, but the tracking speed of the signal will be lost. Therefore, for the signal system with high tracking precision requirements, the parameter ξ can be appropriately increased. The tracking signal after the steady state can be taken to solve the parameters such as phase and frequency. For signal systems with high real-time requirements, the parameters ξ are appropriately reduced.

Combining Section 3.1 and this section, the parameters γ and ξ have a significant impact on the tracking signal. To this end, the signal tracking simulation is conducted under different parameters γ and ξ. Obtain the identification time at which the steady-state error is reduced to 0.5 Hz. The simulation results are shown in Fig. 6. As can be seen from the figure, the rate of identification increases with the increase of γ and decreases with the increase of ξ. Therefore, for different system signals, the tracking requirements can be met by adjusting the parameters.

4. SIMULATION ANALYSIS

A mathematical model was developed to evaluate the effectiveness of the ANF algorithm for solving the phase and

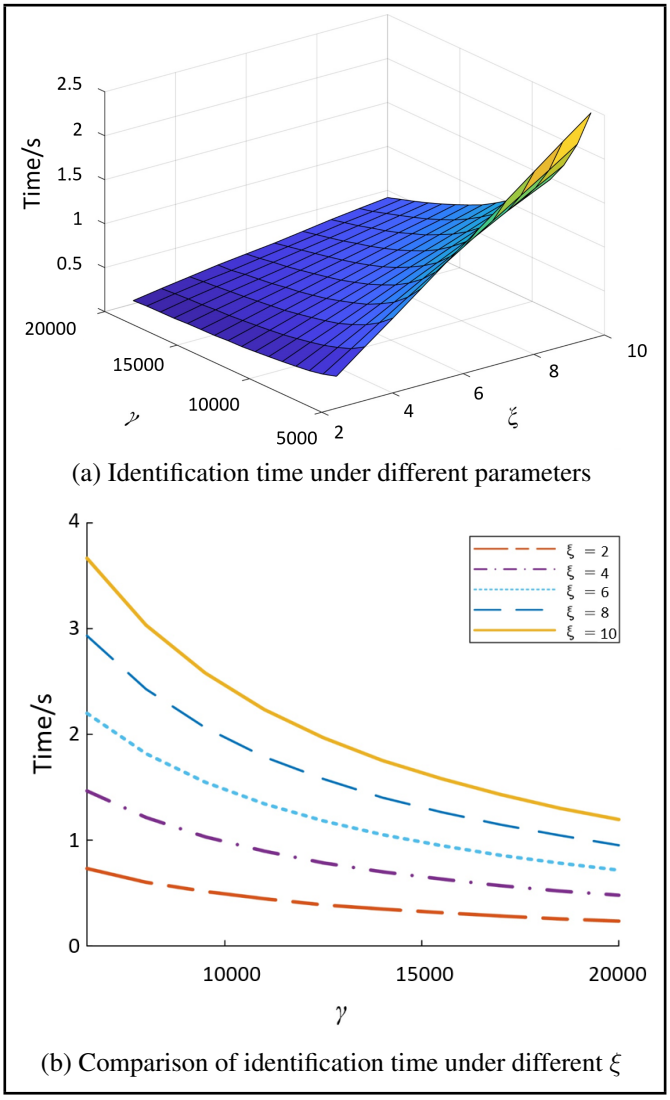

Figure 6. Parameters influence of ANF.

frequency of sinusoidal signals in rotating machinery. Subsequently, simulations are performed on the signal frequency and phase. To simulate the sinusoidal signals of rotating machinery, the simulation model of the magnetic bearing rotor was built, and the frequency and phase of the two quadrature signals were solved.

4.1. Frequency and Phase Solution of a Single Sinusoidal Signal

Equation (8) describes a sinusoidal signal:

$$u(t) = 0.5 \times \sin(50 \times 2\pi t + \pi/3). \tag{8}$$

In the Eq. (8), the frequency of the signal $u(t)$ was 50 Hz and the phase was 60°. Using the structure shown in Fig. 3 (a) to solve the signal frequency and phase, the results are shown in Fig. 7. The input signal can be accurately tracked without phase lag.

Figure 7(a) shows the original signal, the tracking signal and the quadrature signal obtained by the solution. Figure 7(b) solves the sinusoidal signal phase, with a phase range of $-180°$ to 180°.

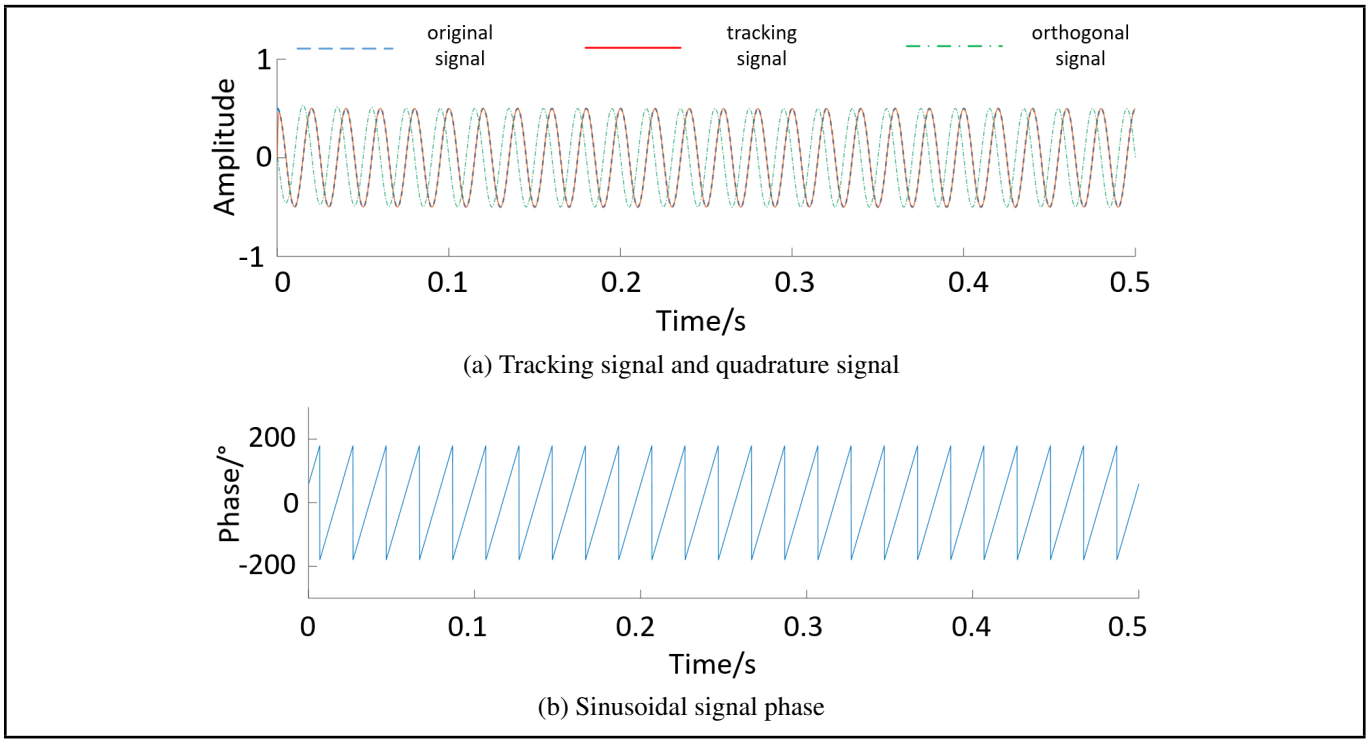

(a) Tracking signal and quadrature signal

(b) Sinusoidal signal phase

Figure 7. Phase solution of single sinusoidal signal.

4.2. Frequency and Phase Difference Solution of Two Sinusoidal Signals

Equations (9) and (10) describe two sinusoidal signals with same frequency and amplitude and different phase:

$$u_1(t) = A_1 \times \sin(\omega \times 2\pi t + \varphi_1); \tag{9}$$

$$u_2(t) = A_2 \times \sin(\omega \times 2\pi t + \varphi_2); \tag{10}$$

where ω was the frequency, A_1 and A_2 were the amplitudes of signals $u_1(t)$ and $u_2(t)$, φ_1 and φ_2 were the initial phases, respectively. Here, A_1 and A_2 were both 0.5, φ_1 and φ_2 were $60°$ and $0°$, respectively.

According to the definition of phase difference, the phase difference between signals $u_1(t)$ and $u_2(t)$ is as follows.

$$\varphi_0 = \varphi_2 - \varphi_1. \tag{11}$$

Using the structure shown in Fig. 3(b), the phase of signals $u_1(t)$ and $u_2(t)$ were respectively solved, and the phase difference between the two signals was obtained. The results are shown in Fig. 8. Figure 8(a) is a time domain diagram of signal 1 and signal 2, and Fig. 8(b) is a phase spectrum obtained by solving signal 1 and signal 2.

To further verify the feasibility of the method in this paper, two signals with different frequencies, amplitudes and phase differences are solved in this paper. Detailed information of each signal is shown in Table 1. The comparison results after reaching the steady state are shown in Fig. 9. As can be seen from Table 1, for simulation signals of different frequencies and amplitudes, the solution results can reach zero error.

4.3. Simulation of Magnetic Bearing Rotor Displacement Signal

To verify the feasibility of this method for solving the frequency and phase of the rotating machinery displacement signal, a dynamic model of the four degrees of freedom magnetic bearing rotor system[17] was built. The rotor rotation and displacement signals were collected and simulated. The frequency and phase of the displacement signal were solved.

Table 1. Comparison of signal information and solution results.

Group	1	2	3	4
Frequency	10 Hz	15 Hz	20 Hz	25 Hz
Amplitude	0.9	0.7	0.5	0.3
Phase difference	30°	60°	90°	120°
Error	0	0	0	0

The magnetic bearing rotor system has two radial magnetic bearings and one axial magnetic bearing. This paper mainly studies the radial sinusoidal vibration signal of the rotor. Therefore, the dynamic model of the radial rotor four degree of freedom was established below as Eq. (12). The magnetic bearing rotor was slender, with two ends, designated as a-end and b-end. Displacement sensors were arranged at orthogonal positions at both ends of the rotor, which can monitor the displacement signal of the rotor in real time. The schematic diagram of the magnetic bearing rotor is shown in Fig. 10.

$$\begin{bmatrix} \frac{ml_b}{l} & \frac{ml_a}{l} & 0 & 0 \\ -\frac{J}{l} & \frac{J}{l} & 0 & 0 \\ 0 & 0 & \frac{ml_b}{l} & \frac{ml_a}{l} \\ 0 & 0 & -\frac{J}{l} & \frac{J}{l} \end{bmatrix} \begin{bmatrix} \ddot{x}_a \\ \ddot{x}_b \\ \ddot{y}_a \\ \ddot{y}_b \end{bmatrix} + \omega \begin{bmatrix} 0 & 0 & 0 & 0 \\ 0 & 0 & -\frac{J_z}{l} & \frac{J_z}{l} \\ 0 & 0 & 0 & 0 \\ -\frac{J_z}{l} & \frac{J_z}{l} & 0 & 0 \end{bmatrix} \begin{bmatrix} \dot{x}_a \\ \dot{x}_b \\ \dot{y}_a \\ \dot{y}_b \end{bmatrix} =$$
$$\begin{bmatrix} k_x & k_x & 0 & 0 \\ -\frac{k_x}{l_a} & \frac{k_x}{l_b} & 0 & 0 \\ 0 & 0 & k_x & k_x \\ 0 & 0 & -\frac{k_x}{l_a} & \frac{k_x}{l_b} \end{bmatrix} \begin{bmatrix} x_a \\ x_b \\ y_a \\ y_b \end{bmatrix} + \begin{bmatrix} k_i & k_i & 0 & 0 \\ -\frac{k_i}{l_a} & \frac{k_i}{l_b} & 0 & 0 \\ 0 & 0 & k_i & k_i \\ 0 & 0 & -\frac{k_i}{l_a} & \frac{k_i}{l_b} \end{bmatrix} \begin{bmatrix} i_{ax} \\ i_{bx} \\ i_{ay} \\ i_{by} \end{bmatrix}; \tag{12}$$

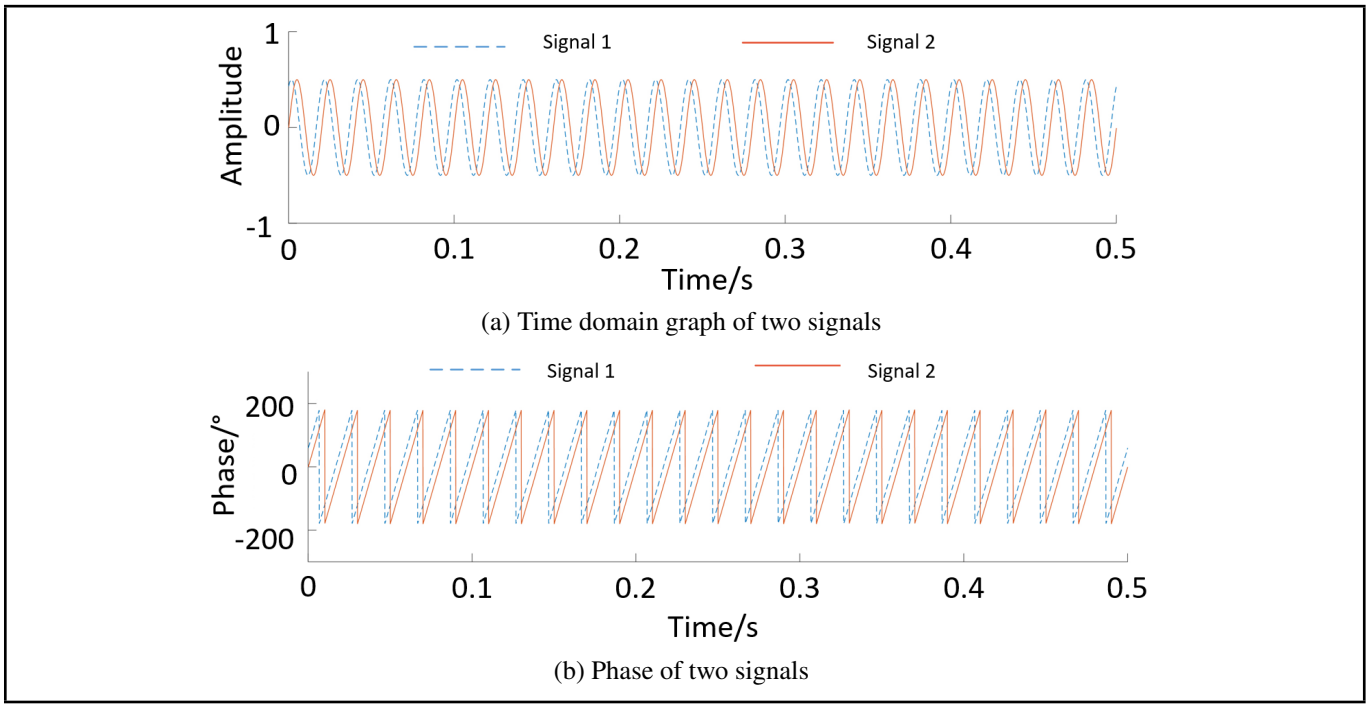

Figure 8. Phase difference solution of two sinusoidal signals.

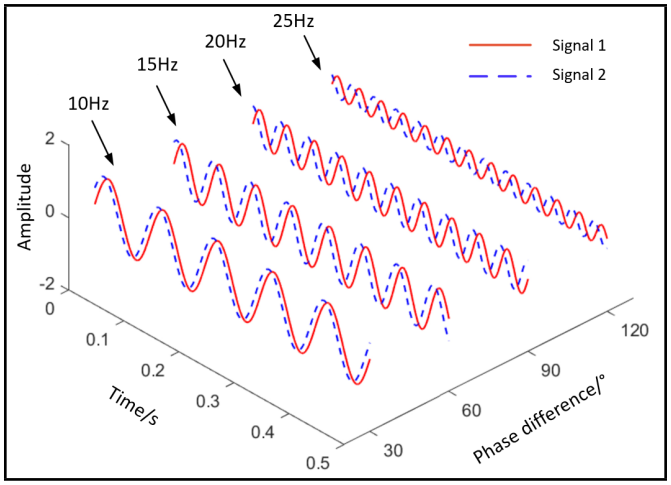

Figure 9. Phase difference solution of two sinusoidal signals with different frequencies.

where k_i was the current stiffness coefficient, k_x was the displacement stiffness coefficient, l_a was the distance from the a-end magnetic bearing to the rotor centroid, l_b was the distance from the b-end magnetic bearing to the rotor centroid, l was the distance between the two ends of the bearing, m was the rotor mass, J was the moment of inertia about the x and y axes, and J_z was the moment of inertia about the z axis. The specific parameters of the magnetic bearing rotor model used in this paper are shown in Table 2.

Table 2. Magnetic bearing rotor related parameters.

Parameter	Value	Unit
Distance from a-end magnetic bearing to rotor centroid l_a	70.17	mm
Distance from b-end magnetic bearing to rotor centroid l_b	53.63	mm
Distance between the two ends of the bearing l	123.8	mm
Rotor mass m	5.8	kg
Inertia about x and y axes J	$4.2e^{-2}$	kgm^2
Inertia about the z axis J_z	$2.8e^{-3}$	kgm^2
Current stiffness coefficient k_i	142.1	N/A
Displacement stiffness coefficient k_x	472589.0	N/m

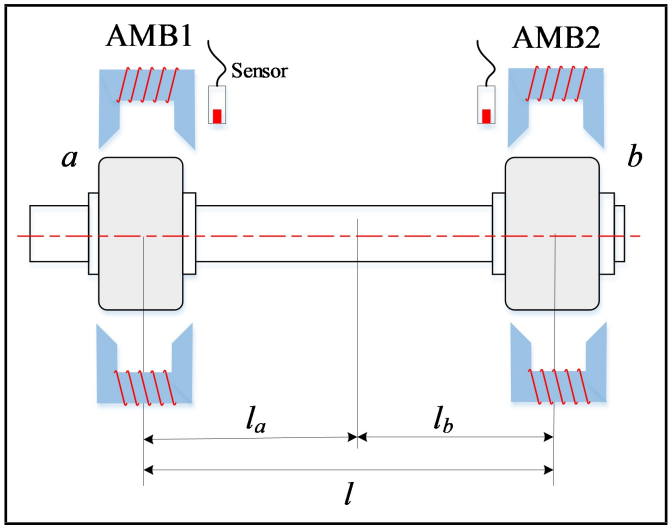

Figure 10. Schematic diagram of the magnetic bearing rotor.

Based on the above dynamic model and the magnetic bearing rotor parameter, the simulation model of the magnetic bearing rotor system was built. The schematic diagram of magnetic bearing rotor system is shown in Fig. 11. It mainly included controller, power amplifier, displacement sensor, magnetic bearing, rotor and other structures. The ANF was used to process displacement signals or control current signals, obtaining basic information such as frequency and phase to achieve real-time monitoring of the system.

Based on the simulation model of the magnetic bearing rotor, the rotation speed of 30 Hz was simulated. The rotor displacement signal was collected, and the frequency and phase of each of the two orthogonal displacement signals are obtained. The analysis results are shown in Fig. 12.

It can be seen from Fig. 12(b) that the solution frequency basically stabilizes at 30 Hz after 0.2 s. As can be seen from Fig. 12(d), after 0.2 s, the phase difference solution results coincide with the 90° reference line. The results verify the fea-

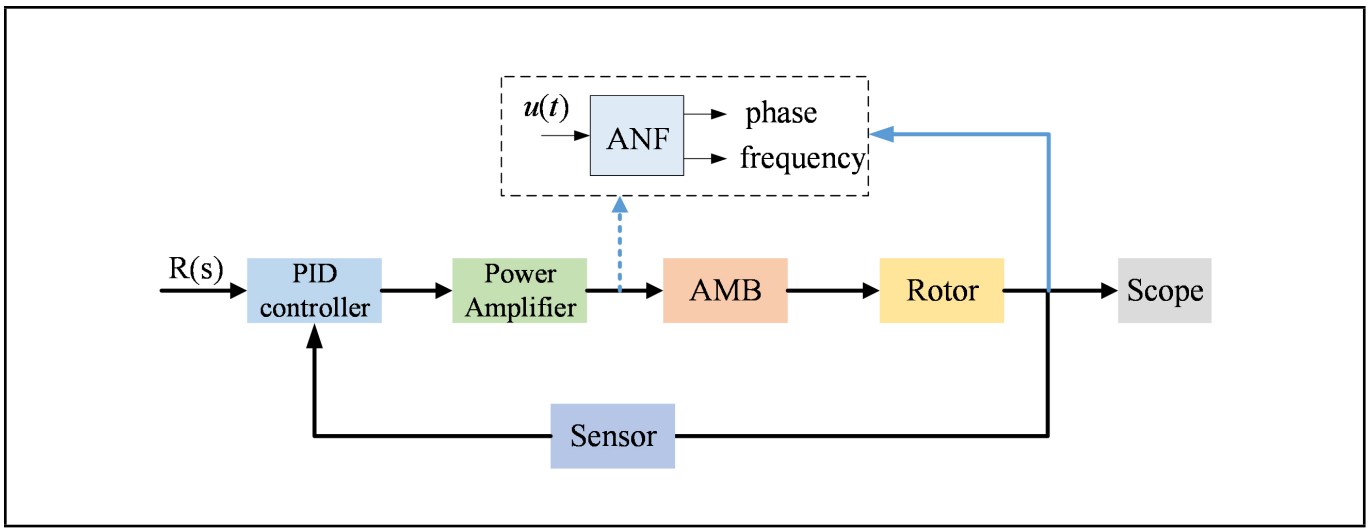

Figure 11. Schematic diagram of magnetic bearing rotor system.

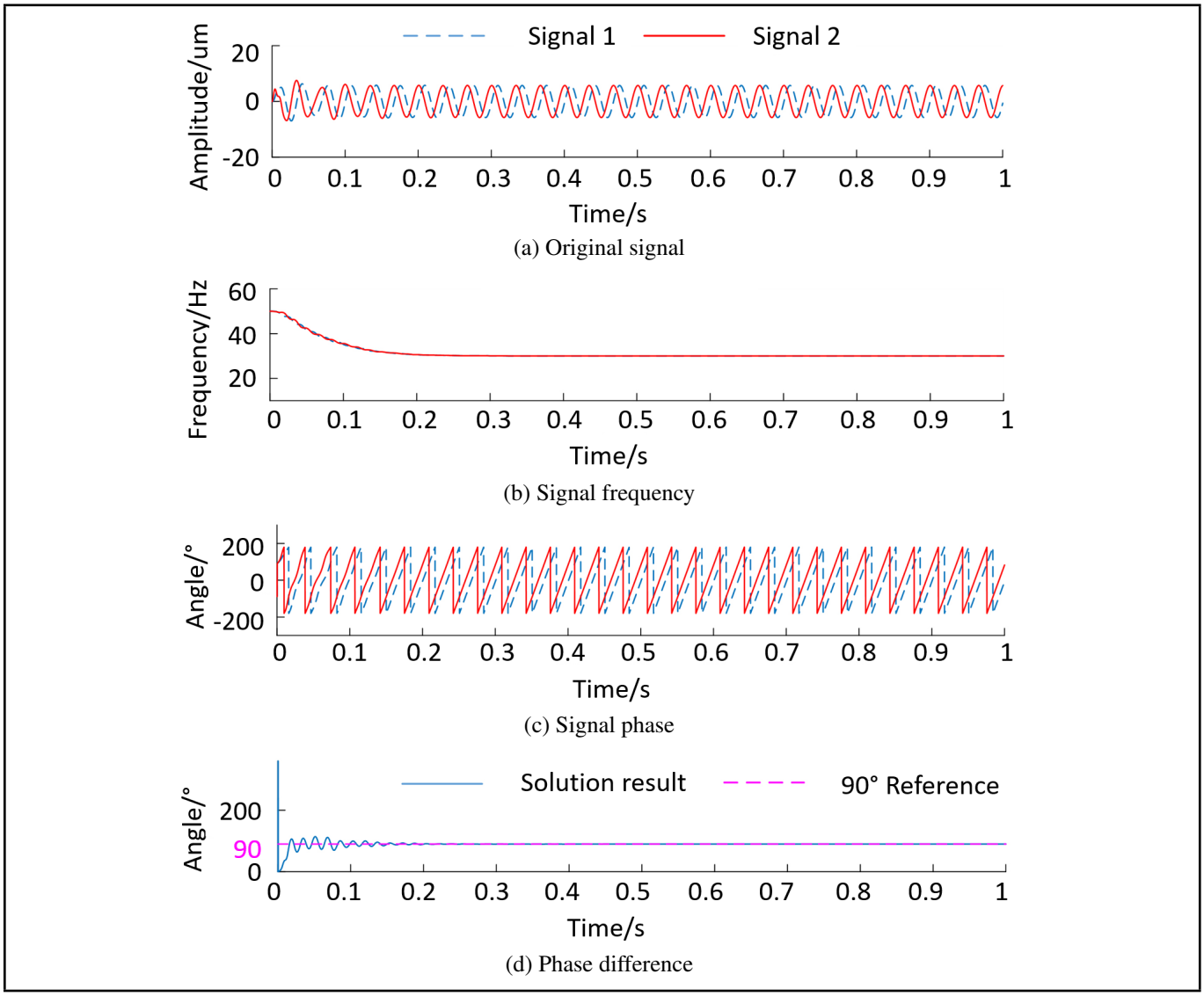

Figure 12. Results of simulation signal tracking and phase solution for magnetic bearing rotor.

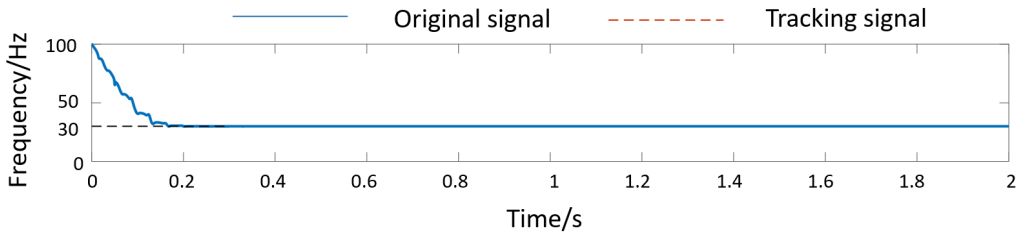

(a) Calculation of fundamental frequency

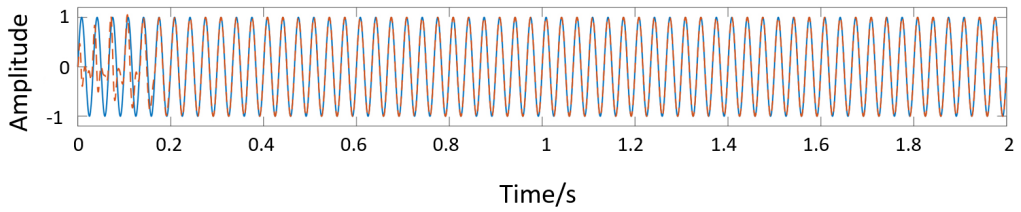

(b) Fundamental frequency signal tracking

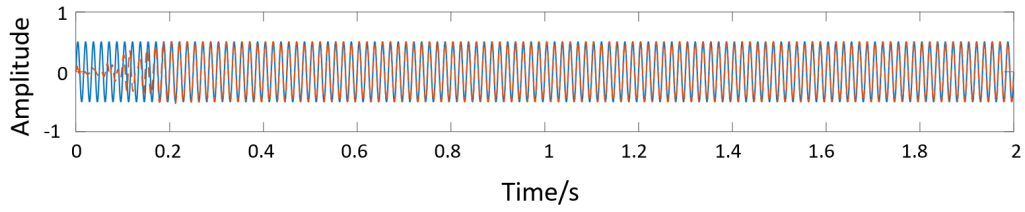

(c) Second harmonic signal tracking

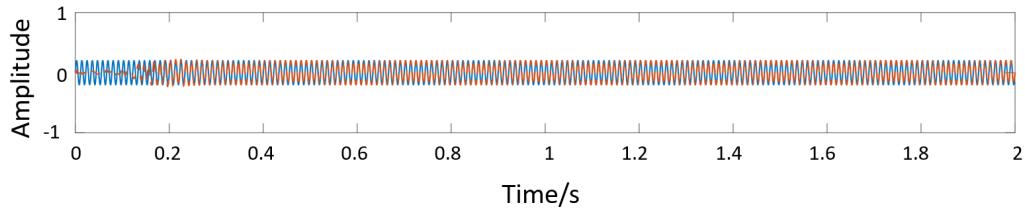

(d) Third harmonic signal tracking

Figure 13. Frequency tracking results for signals with harmonic components.

sibility of the method for solving the displacement signal frequency and phase of rotating machinery.

4.4. Tracking of Multi-Harmonic Signal

To verify the tracking effect of ANF on multi-harmonic signals, the tracking verification of the signals was carried out based on the ANF connected in parallel in Fig. 2.

Take the input signal as follows:

$$u'(t) = \sin(30 * 2\pi t) + 0.5 * \sin(60 * 2\pi t) + 0.2 * \sin(90 * 2\pi t). \quad (13)$$

The fundamental frequency was 30 Hz, the amplitude is 1, the amplitude of the second harmonic is 0.5, and the amplitude of the third harmonic is 0.2. As shown in Fig. 13, it is the frequency solution result and the tracking result of each frequency signal. It can be seen from the figure that after 0.2 s, stable tracking of the fundamental frequency signal and the harmonic frequency signal can be basically achieved, as well as accurate solution of the fundamental frequency.

5. EXPERIMENTAL RESEARCH

As shown in Fig. 14(a), two displacement sensors were arranged at both ends of the rotor. Figure 14(b) is a schematic diagram of the displacement sensors arrangement. The experimental signals were collected on the magnetic bearing rotor test rig. There was an imbalance on the magnetic suspension rotor, which generated centrifugal force on the rotor and generates vibration when the rotor rotated and worked. The displacement signal collected by the sensor was a sinusoidal signal.

Due to the orthogonal arrangement of displacement sensors 1 and 2. Theoretically, the displacement signal at sensor 2 was 90° ahead of the displacement signal at sensor 1.

The rotor speed was stabilized at 70 Hz, and the sensor was used for signal acquisition. The displacement signal was analyzed based on ANF, and the analysis result is shown in Fig. 15. Figure 15(a) shows the original signal collected by the displacement sensors and the tracking signal of the ANF. The original signal contains sinusoidal signals corresponding to the relevant frequencies and noises. Figure 15(b) shows the signal frequency identified by the ANF. It can be seen from the figure that after 0.3 s, it is basically approaching 70 Hz. Fig-

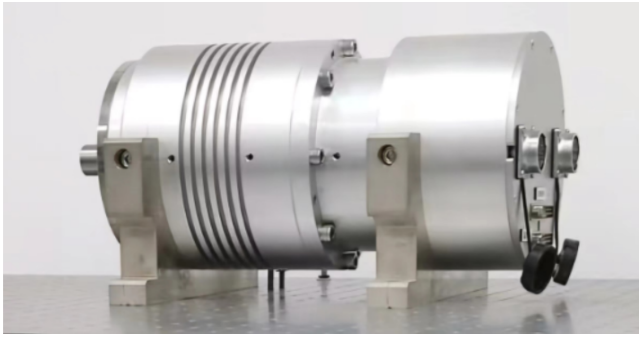

(a) Magnetic bearing rotor test rig

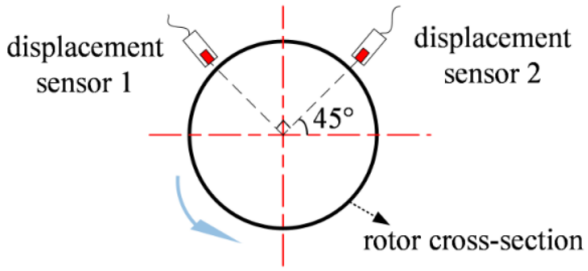

(b) Installation position of displacement sensors

Figure 14. The test rig and the installation position of displacement sensors.

ure 15(c) shows the phase of the two signals. Figure 15(d) shows a phase difference between the two signals. Due to the existence of harmonics and noise, there are some fluctuations in the phase difference signal, but it is basically stable at around 90°. The average value of the phase difference signal after 0.5 s is 90.9°, which is consistent with the theoretical value of 90°. This slight deviation may be caused by various factors such as mechanical assembly or signal acquisition.

6. CONCLUSION

Aiming at the problem of solving the frequency and phase of rotating machinery sinusoidal signal, the research on the frequency and phase solution method based on ANF is carried out. The main conclusions are as follows.

1. The ANF can accurately solve the frequency and phase of the rotating machinery sinusoidal signal, providing a new idea for the solution of the phase and frequency.

2. In ANF system, the parameters γ and ξ have influence on the tracking speed and tracking accuracy of the signal. The parameters can be adjusted appropriately according to the needs of signal solution.

3. The identification method based on ANF can achieve zero error for the simulated signal. There is a deviation between the solution result of the experimental signal and the theoretical value, but the deviation is not caused by the calculation method. This deviation may be due to various factors such as the angle at which the sensor is installed and the other mechanical assembly.

ACKNOWLEDGEMENTS

This work has been supported by National Natural Science Foundation of China (52205050), the Intelligent Manufacturing Longcheng Laboratory (CJ20242057), Postgraduate Research & Practice Innovation Program of Jiangsu Province (KYCX25_3395).

REFERENCES

[1] Alegria, F. A., Xie, L. and Pasadas, D. Study of the bias of the initial phase estimation of a sinewave of known frequency in the presence of phase noise, *Sensors*, **24**(12), 3730, (2024). https://doi.org/10.3390/s24123730

[2] Yang, M., Huang, H., Liu, Z., Cai, C., Wang, Y. and Yang, J. Sine approximation-based comparison method for determining the phase–frequency characteristic of analog-to-digital converters, *IEEE Transactions on Industrial Electronics*, **71**(2), 2142–2145, (2023). https://doi.org/10.1109/TIE.2023.3253953

[3] Miao, H. Adaptive filter design for cyclostationary processes associated with sine-wave extraction operation, *Digital Signal Processing*, **154**, 104698, (2024). https://doi.org/10.1016/j.dsp.2024.104698

[4] Duan, X. and Feng, Z. Time-varying filtering for nonstationary signal analysis of rotating machinery: Principle and applications, *Mechanical Systems and Signal Processing*, **192**, 110204, (2023). https://doi.org/10.1016/j.ymssp.2023.110204

[5] Saber, M. and Elkenawy, E. M. Design and implementation of accurate frequency estimator depend on deep learning, *International Journal of Engineering and Technology*, **9**(2), 367–377, (2020). https://doi.org/10.14419/ijet.v9i2.30473

[6] Singh, A. and Parida, S. K. Power system frequency and phasor estimation for a low-cost synchro phasor device using the nonlinear least-square method, *IEEE Transactions on Industry Applications*, **58**(1), 39–48, (2021). https://doi.org/10.1109/TIA.2021.3117932

[7] Guan, X., Zhou, J., Jin, C., Wu, H. and Lin, Y. Adaptive surge detection of magnetic suspension centrifugal blower based on rotor radial displacement signal and SOGI-FLL with prefilter, *Measurement Science and Technology*, **33**(6), 065304, (2022). https://doi.org/10.1088/1361-6501/ac5a9a

[8] Guan, X., Zhou, J., Jin, C. and Lin, Y. Surge detection of magnetic suspension fluid machinery based on rotor axial displacement signal and normalized second-order generalized integrator-frequency locked loop with prefilter, *Journal of Vibration and Control*, **29**(21–22), 4935–4947, (2023). https://doi.org/10.1177/10775463221127479

[9] Magron, P. and Virtanen, T. Online spectrogram inversion for low-latency audio source separation, *IEEE Signal Processing Letters*, **27**, 306–310, (2020). https://doi.org/10.1109/LSP.2020.2970310

[10] Mayer, F., Williamson, D. S., Mowlaee, P. and Wang, D. L. Impact of phase estimation on single-channel speech separation based on time-frequency masking, *The Journal of the Acoustical Society of America*, **142**, 4668–4679, (2017). https://doi.org/10.1121/1.4986647

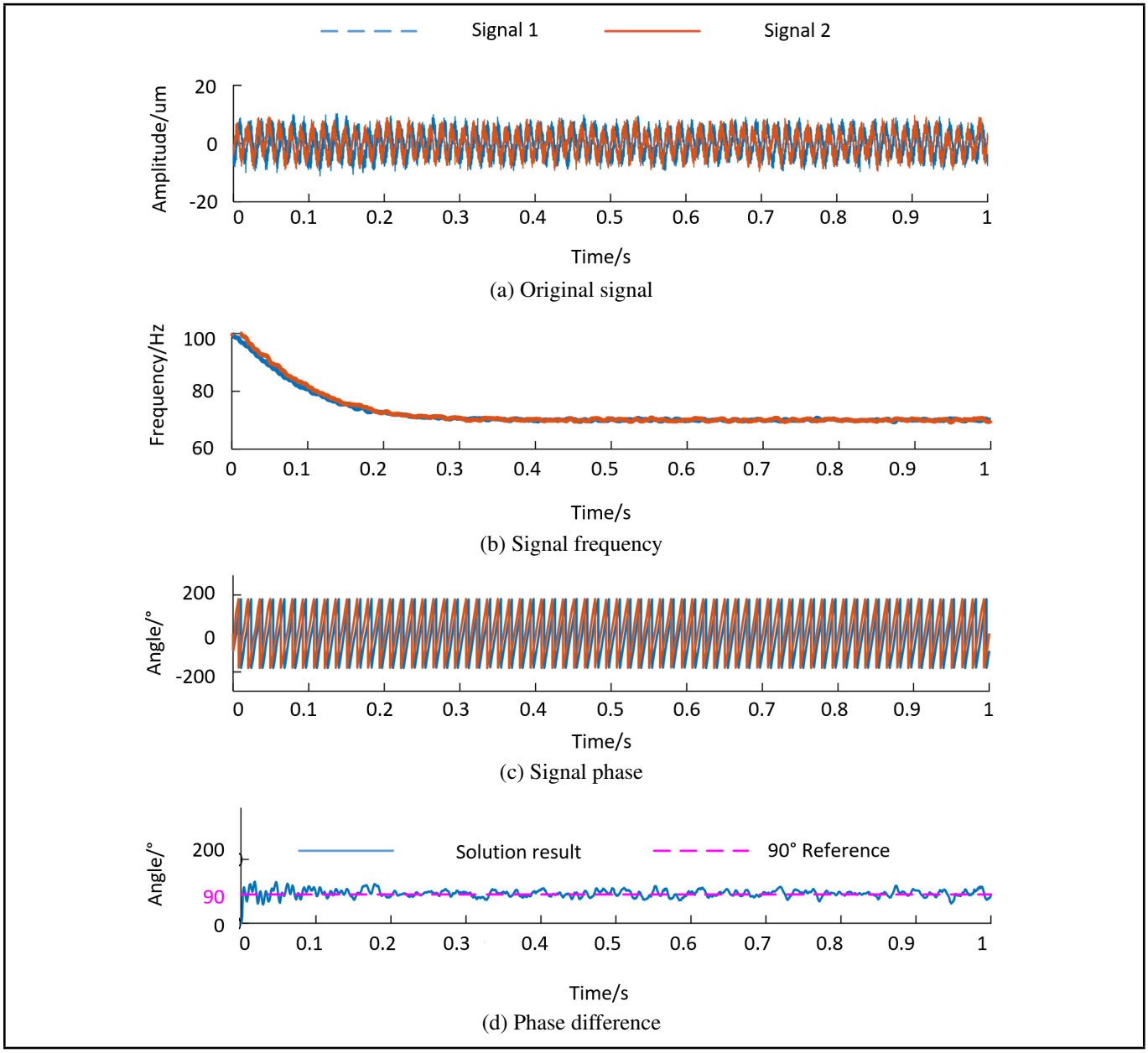

Figure 15. Experimental signal analysis results.

[11] Zhang, M., Tang, J., Zhou, J., Han, X. and Wang, K. Vibration suppression of multi-stage-blade AMB-rotor using parallel adaptive and cascaded multi-frequency notch filters, *Applied Sciences*, **14**, 6255, (2024). https://doi.org/10.3390/app14146255

[12] Ma, W., Liu, G., Zhou, J., Han, X. and Zheng, S. Surge detection of AMB-supported centrifugal compressors using a normalized adaptive notch filter, *IEEE Transactions on Instrumentation and Measurement*, **73**, 1–10, (2024). https://doi.org/10.1109/TIM.2024.3372218

[13] Mojiri, M., Karimi-Ghartemani, M. and Bakhshai, A. Time-domain signal analysis using adaptive notch filter, *IEEE Transactions on Signal Processing*, **55**(1), 85–93, (2006). https://doi.org/10.1109/TSP.2006.885686

[14] Wang, Q., Gu, X. and Lin, J. Adaptive notch filter design under multiple identical bandwidths, *AEU – International Journal of Electronics and Communications*, **82**, 202–210, (2017). https://doi.org/10.1016/j.aeue.2017.08.054

[15] Guan, X., Zhang, J., Yu, S., Peng, H. and Sun, L. Misalignment vibration compensation of magnetic suspension multi-span rotors based on phase-shift notch filter, *Measurement Science and Technology*, **37**(12), 126202, (2026). https://doi.org/10.1088/1361-6501/ae5281

[16] Guan, X., Li, H., Zhu, S., Lu, Z., She, S. and Liu, T. Misalignment fault detection of magnetic suspension multi-span rotors based on improved adaptive notch filter, *Journal of Vibration and Control*, (2025). https://doi.org/10.1177/10775463251397323

[17] Bian, X., Shi, Z., Sun, Z., Zhao, J., Liu, X., Yan, X. and Mo, N. Synchronous disturbance suppression of active magnetic bearing rotor systems using variable period adaptive control algorithm, *Measurement Science and Technology*, **35**(1), 015906, (2024). https://doi.org/10.1088/1361-6501/ad02b4